# Fruit-FIT: Drone Interfaced Multiplexed Sensor Suite to Determine the Fruit Ripeness

Nafize Ishtiaque Hossain<sup>1</sup> and Shawana Tabassum<sup>1</sup>\*

<sup>1</sup>Electrical Engineering, The University of Texas at Tyler, Tyler, TX, United States of America \*Corresponding author: stabassum@uttyler.edu

Abstract—This work presents a hybrid sensor suite comprising a microneedle-based multiplexed hormone sensor and a volatile organic compound sensor integrated on a single chip. The microneedle sensors measured two phytohormones, salicylic acid and indole-3-acetic acid levels with onboard pH correction, and the volatile organic compound sensor measured the gaseous hormone ethylene. The sensor suite was deployed through a drone on ripe and unripe bell peppers before harvest. Dynamic measurement of salicylic acid, indole-3-acetic acid, and ethylene gas in bell peppers informed the progression of ripening, which will be pivotal in determining the optimum time to harvest and reducing postharvest losses.

Keywords—microneedle sensor, electrochemical sensor, salicylic acid, indole-3-acetic acid, ethylene, drone interface.

#### I. INTRODUCTION

The postharvest qualities of fruits and vegetables depend not only on postharvest management practices but also on preharvest monitoring and treatment [1]. Fruits and vegetables that are inappropriately maintained before harvest, can never be improved in quality by any postharvest treatment [2]. Therefore, it is imperative to investigate and control the preharvest factors that are directly associated with the quality of the harvest. Monitoring the progression of fruit ripening is crucial to obtaining optimal fruit quality and determining the time to harvest. Ripening is a complex process governed by a myriad of factors including hormonal balance. Although the critical role of hormones in fruit development has been well established, previous research was mostly centered around how singular hormones affect fruit ripening. For instance, an upsurge in ethylene production is observed in climacteric fruits such as tomatoes and bananas [3, 4], while a progressive accumulation of the phytohormone abscisic acid is reported in non-climacteric fruits/vegetables such as grapes and bell peppers [5, 6]. However, recent investigations reveal that a complex network of hormonal balance and their crosstalk regulates the ripening process [7]. Research has also shown that endogenous salicylic acid (SA) and indole-3-acetic acid (IAA) play multiple roles in fruit development and ripening. For instance, their levels are generally higher during the initial phases of fruit development and subside progressively at later stages [8].

However, the transport of these hormones and their dynamic interplay in fruits/vegetables remain much less explored and need further investigation. This knowledge gap is primarily due to the lack of integrated sensors that can provide fruit hormonal measurements *in situ*. The traditional methods to assess the quality and maturity of fruits and vegetables include infrared spectroscopy, imaging and

machine vision, and electronic noses [9]. Although these methods provide non-destructive and multiplexed analysis of several internal attributes of the fruit/vegetable, they are discrete, bulky, manually operated, lack spatiotemporal information, and often effective at later stages of ripening. In contrast to the electrochemical sensors reported in the literature [10, 11], our group presented for the first time stem-[12] and leaf-mounted microneedle sensors [13] for measuring hormone levels *in situ*.

This work presents an advancement of our previous work by proposing a drone-interfaced hybrid sensor suite for measuring gaseous and liquid phytohormones on a single platform to monitor fruit ripeness and maturity. In addition, an onboard pH sensor was incorporated to correct SA and IAA measurements. The hormonal variations in ripe and unripe bell peppers were revealed. The sensor suite was developed using a low-cost fabrication procedure, thereby enabling wide adoption of this automated system for preharvest as well as postharvest quality control.

#### II. SENSOR SUITE DESIGN

#### A. Electrode Fabrication

The proposed sensor suite was made of five arrays of microneedles. One array worked as the shared reference electrode (RE), one as the shared counter electrode (CE), and the other three arrays served as working electrodes for SA, IAA and pH sensors (namely WEsA, WEIAA, and WEpH, respectively). A 4cm x 3cm x 0.8cm box was designed with an open ceiling and three sidewalls, as depicted in Fig. 1a. The ethylene sensor was placed inside a chamber enclosed by the three sidewalls, whereas the microneedle sensors were laid on top of the sidewalls. Each microneedle array consisted of eight pyramid-shaped microneedles, each having a square base of 800 µm, a height of 800 µm, and a tip angle of 60°. The Form 3B stereolithography printer was used to print the 3D box with the microneedles. BioMed Clear resin was used as the printing material to ensure biocompatibility of the microneedles.

The ethylene sensor was fabricated by a screen printing process, as shown in Fig. 1b and described in more detail elsewhere [14]. A thin Nafion sheet was used as the substrate material because it works as a solid-state electrolyte. Briefly, Nafion was covered with a transfer tape that worked as the stencil mask (Fig. 1b-i). A benchtop cutter generated the electrode patterns on the transfer tape (Fig. 1b-ii). Next, the reference electrode was coated with Ag/AgCl paste, while the working electrode (WE<sub>ET</sub>) and the counter electrode (CE) were coated with graphene ink (Fig. 1b-iii-v). The electrodes

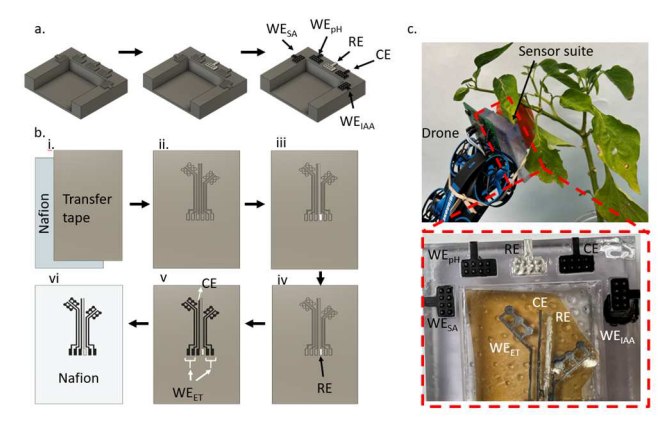


Fig. 1. Step-by-step fabrication of the electrodes. (a) The 3D printed microneedle electrodes. (b) Screen printing of ethylene sensor: i. Nafion sheet covered with a transfer tape, ii. electrode patterns cut by a benchtop cutter, iii. transfer tape from the reference electrode region was removed, iv. reference electrode was printed with Ag/AgCl paste, v. working and counter electrode areas were exposed and printed with graphene ink, vi. the transfer tape was removed resulting in electrodes transferred o the Nafion sheet. (c) Optical image of the sensor suite interfaced with a drone. The expanded image shows the top view of the box.

were cured at 80°C for 60 minutes followed by separation of the transfer tape from the Nafion sheet (Fig. 1b-vi). The ethylene sensor had a dual working electrode (see Fig. 1b-v), which significantly enhanced the sensitivity to sub-ppm ethylene.

### B. Synthesis of SA and IAA Selective Coatings

The working electrode of the SA sensor,  $WE_{SA}$ , was functionalized by a copper metal-organic framework (CuMOF)/nafion/carbon black nanocomposite. The detailed preparation procedure of this coating is described in our previous report [14].  $4\mu L$  of the nanocomposite solution was drop cast on  $WE_{SA}$  and dried at room temperature.

The IAA working electrode, WE<sub>IAA</sub>, was modified with gold nanoparticles decorated graphene hydrogel nanocomposite. The coating preparation procedure is detailed in [13, 15].  $4\mu L$  of the as-prepared solution was drop cast on WE<sub>IAA</sub>.

### C. Synthesis of Ethylene Selective Coating

WE<sub>ET</sub> was functionalized with a composite copper complex (I)-single-walled carbon nanotube coating for selective measurement of ethylene gas following the recipe in [16, 17]. 4  $\mu$ L of this solution was drop cast on WE<sub>ET</sub>.

# D. Synthesis of pH Selective Coating

 $WE_{pH}$  was modified with polyaniline (PANI) nanofibers via electrodeposition, as detailed in [18]. The pH sensor electrodes were immersed in a mixture of 0.1M aniline and 0.1M HCl followed by 85 cycles of cyclic voltammetry (CV) for -0.2V to 0.6V at a 50mV/s scan rate.

### III. RESULTS AND DISCUSSION

#### A. Electrochemical Detection of SA, IAA, and Ethylene

To perform the electrochemical measurements, differential pulse voltammetry (DPV) was conducted in a

This work was supported in part by VentureWell Grant No. 21716-20 and in part by the National Science Foundation Award No. 2138701.

potential range from -1.0V to 1.2V for SA and from 0.2V to 1.2V for IAA. The SA sensor was calibrated for SA levels ranging from 50  $\mu M$  to 1000  $\mu M$ , while the IAA sensor was calibrated for IAA levels varying from 0.1  $\mu M$  to 200  $\mu M$ , commensurate with the typical SA and IAA concentrations found in plants [14, 15]. Fig. 2 shows the DPV responses and the resulting calibration plots for the two hormone sensors. A ratiometric approach was used to calibrate the SA sensor, meaning the ratio of SA and CuMOF redox current peaks (I\_{SA}/I\_{CuMOF}) was plotted as a function of SA concentration and a power series curve was fitted to the data points (Fig. 2b). The SA and IAA sensors exhibited sensitivities of 0.005  $\mu M^{-1}$  and 0.8325  $\mu A$   $\mu M^{-1}$ , with the limit of detection being 0.93  $\mu M$  and 0.08  $\mu M$ , respectively.

Cyclic Voltammetry (CV) method was used to conduct electrochemical characterization of the ethylene sensor. Different concentrations of ethylene gas were generated by controlling the gas flow rate and time in a flow chamber.

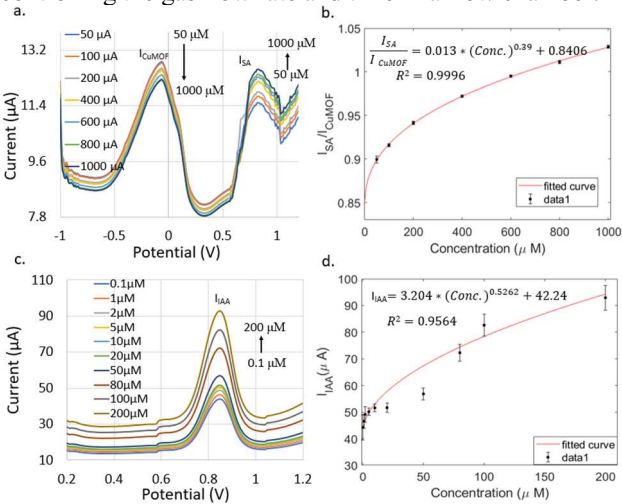


Fig. 2. (a) Differential Pulse Voltammetry (DPV) responses for different concentrations of SA. (b) SA calibration curve showing  $I_{SA}/I_{CuMOF}$  vs. SA concentrations. (c) DPV responses for different concentrations of IAA. (d) IAA calibration curve showing  $I_{IAA}$  vs. IAA concentrations.

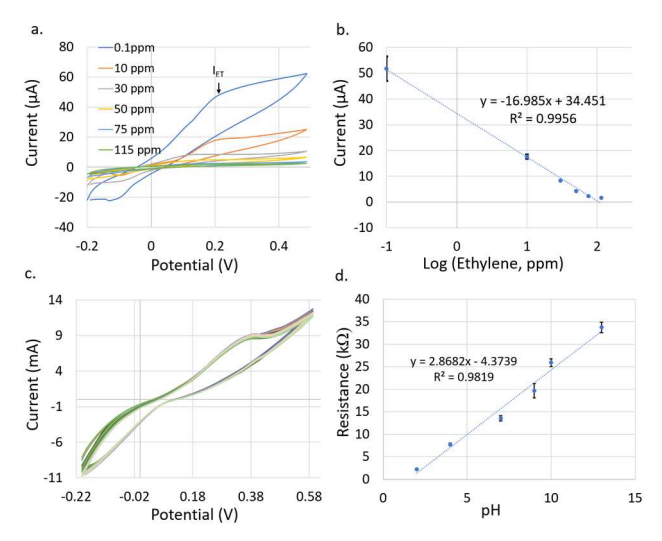


Fig. 3. (a) Cyclic Voltammetry (CV) responses for different concentrations of ethylene. (b) Ethylene calibration curve showing current vs. ethylene concentrations. (c) CV responses for PANI deposition. (d) pH sensor calibration curve. Error bars represent 3 repeated measurements.

The concentrations ranging from 0.1 ppm to 115 ppm were used to calibrate the ethylene sensor. The CV responses depict that the ethylene oxidation peak current ( $I_{ET}$ ) lies between 0.12V and 0.17V. Upon exposure to a higher concentration of ethylene, the oxidation peak current decreased because ethylene molecules blocked the active sites in the carbon nanotube coating (Fig. 3a-b) [17].

#### B. pH Sensor Characterization

The pH sensor was calibrated with plant sap. The sap pH was varied by adding 0.1M HCl and 0.01M NaOH. The pH sensor demonstrated an increase in the resistance measured across the electrodes with increasing pH value, as is illustrated in Fig. 3d.

# C. Selectivity Test

The SA and IAA sensors were tested against several interfering species typically found in fruits/vegetables [19],

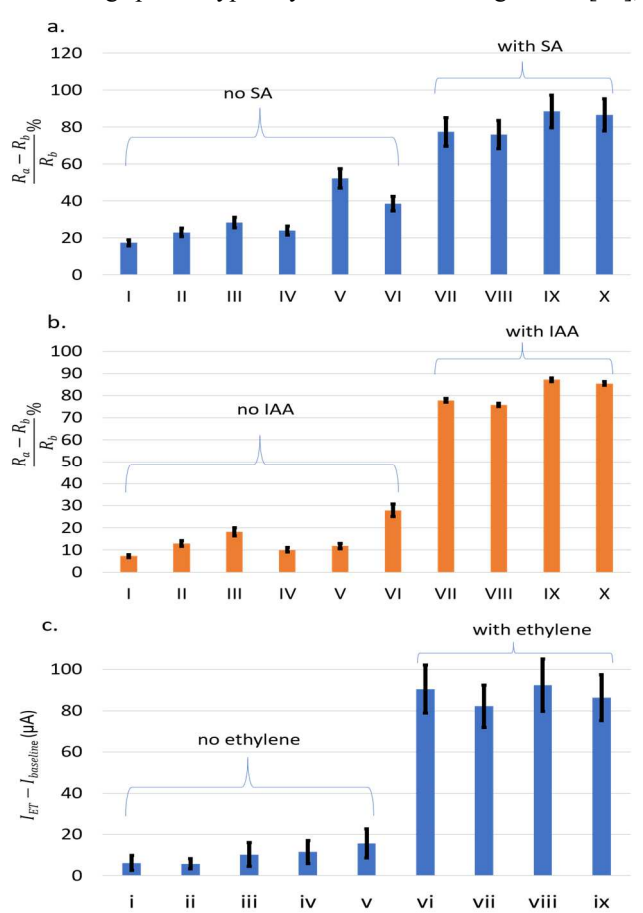


Fig. 4. Selectivity test for (a) SA and (b) IAA sensors. Here, i -x denote the following solutions: (i) Jasmonic acid (JA) = 50μM, (ii) L-Cysteine (L-Cys) =  $50\mu\text{M}$ , (iii) glucose =  $50\mu\text{M}$ , (iv) citric acid =  $50\mu\text{M}$ , (v) ascorbic acid = 50µM, (vi) a mixture of JA, L-Cys, glucose, citric acid, and ascorbic acid (50µM each), (vii) target hormone (SA/IAA) = 100µM, (viii) a mixture of ascorbic acid, JA, L-Cys, glucose, citric acid, ascorbic acid (50µM each), and target hormone =  $100\mu M$ , (ix) target (SA= $900\mu M$  or IAA= $200\mu M$ ), (x) a mixture of ascorbic acid, JA, L-Cys, glucose, citric acid, ascorbic acid (50μM each), and target (SA=900μM or IAA=200μM). (c) Selectivity test for ethylene sensor, where i-ix denote: (i) 50ppm N2, (ii) 50ppm CH4, (iii) 50ppm N<sub>2</sub>O<sub>2</sub>O<sub>3</sub> (iv) 50ppm NH<sub>3</sub>, (v) a mixture of 50ppm of N<sub>2</sub>, CH<sub>4</sub>, N<sub>2</sub>O<sub>3</sub> NH<sub>3</sub> each, (vi) 10ppm ethylene, (vii) a mixture of 50ppm N<sub>2</sub>, CH<sub>4</sub>, N<sub>2</sub>O,  $NH_3$  each and 10ppm ethylene, (viii) 115ppm ethylene and (ix) a mixture of 50ppm  $N_2$ ,  $CH_4$ ,  $N_2O$ ,  $NH_3$  each and 115ppm ethylene.  $R_a = I_{SA}/I_{CuMOF}$ for SA sensor and  $I_{IAA}$  for IAA sensor,  $R_b = I_{baseline}/I_{CuMOF}$  for SA sensor and Ibaseline for IAA sensor.

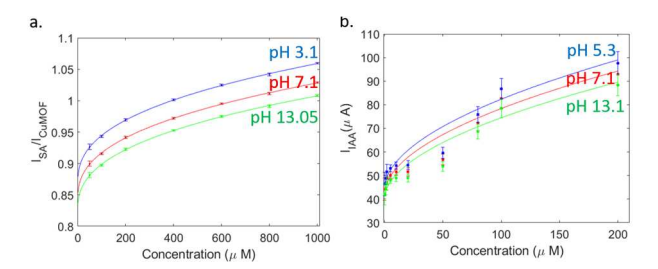


Fig. 5. Calibration curves of (a) SA and (b) IAA sensors for different pH.

while the ethylene sensor was tested against some common interfering gases emitted in an agricultural field [20]. As shown in Fig. 4, all three sensors exhibited negligible responses in the absence of the target analyte, thereby confirming excellent selectivity.

## D. pH Correction of SA and IAA

The SA and IAA values measured with our sensor were corrected for pH variations in bell pepper at different stages of ripening. The pH correction was performed by following the method outlined in [21]. The calibration curves of SA and IAA sensors at different pH values are illustrated in Fig. 5.

#### E. Real-time Monitoring of Fruit Ripening

Bell pepper was selected as the model vegetable for this study. The sensor suite was deployed on bell peppers through a drone (Fig. 1c). The SA, IAA, and ethylene levels were measured once a day for 7 consecutive days (Fig 6a-c). The results show that both SA and IAA levels increased over time in unripe bell pepper, while the levels started to decrease once the bell pepper reached its maturity, which was also observed in previous research [8]. Although the ethylene level showed a rising trend in both ripe and unripe bell peppers, the rate of change was higher in the unripe pepper. Finally, Fig. 6d characterizes the sensor stability over seven days.

#### IV. CONCLUSION AND FUTURE WORK

In summary, this work provides the first demonstration of a drone-interfaced integrated hybrid sensor suite for multiplexed detection of ethylene, SA, and IAA levels with pH correction on a single platform. The sensor was capable of monitoring the varying trend of hormone levels in ripe and unripe bell peppers. Future work will include a comprehensive analysis of these hormones and their crosstalk in a variety of fruits and vegetables.

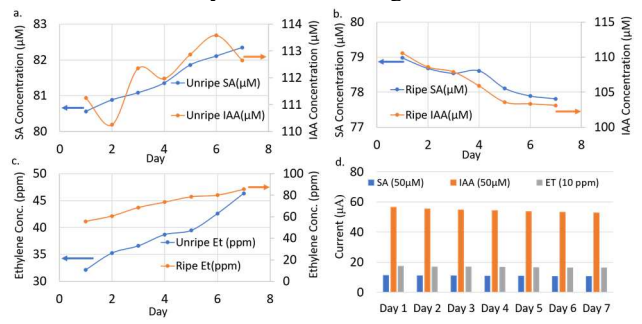


Fig. 6. The trend of SA and IAA in (a) unripe and (b) ripe bell peppers. (c) The trend of ethylene in ripe and unripe bell peppers. (d) Stability analysis of SA, IAA, and ET sensors over one week. Peak current value decreased by 1.15%, 1.33%, and 2.5% for SA, IAA, and ET sensors, respectively.

#### REFERENCES

- I. K. Arah, H. Amaglo, E. K. Kumah, and H. Ofori, "Preharvest and postharvest factors affecting the quality and shelf life of harvested tomatoes: a mini review," Int. J. Agronomy, vol. 2015, pp. 478041, 2015.
- [2] J. M. Harvey, "Reduction of losses in fresh market fruits and vegetables," Annual Review of Phytopathology, vol. 16, no. 1, pp. 321–341, 1978.
- [3] C. S. Barry and J. J. Giovannoni, "Ethylene and fruit ripening," J. Plant Growth Regul., vol. 26, pp. 143–159, 2007. doi: 10.1007/s00344-007-9002-y.
- [4] M. Liu, J. Pirrello, C. Chervin, J.-P. Roustan, and M. Bouzayen, "Ethylene control of fruit ripening: revisiting the complex network of transcriptional regulation," Plant Physiol., vol. 169, pp. 2380–2390, 2015. doi: 10.1104/pp.15.01361
- [5] M. J. Rodrigo, B. Alquezar, and L. Zacarías, "Cloning and characterization of two 9-cis-epoxycarotenoid dioxygenase genes, differentially regulated during fruit maturation and under stress conditions, from orange (Citrus sinensis L. Osbeck)," J. Exp. Bot., vol. 57, pp. 633–643, 2006. doi: 10.1093/jxb/erj048
- [6] S. D. Castellarin, G. A. Gambetta, H. Wada, K. A. Shackel, and M. A. Matthews, "Fruit ripening in *Vitis vinifera*: spatiotemporal relationships among turgor, sugar accumulation, and anthocyanin biosynthesis," J. Exp. Bot., vol. 62, pp. 4345–4354, 2011. doi: 10.1093/jxb/err150
- [7] Y. Li, Y. Lua, L. Lia, Z. Chu, H. Zhang, H. Li, A. R. Fernie, and B. Ouyang, "Impairment of hormone pathways results in a general disturbance of fruit primary metabolism in tomato," Food Chem., vol. 274, pp. 170–179, 2019. doi: 10.1016/j.foodchem.2018.08.026
- [8] A. Oikawa, T. Otsuka, R. Nakabayashi, Y. Jikumaru, K. Isuzugawa, H. Murayama, K. Saito, K. Shiratake, "Metabolic profiling of developing pear fruits reveals dynamic variation in primary and secondary metabolites, including plant hormones," PLoS One, vol. 10, pp. e0131408, 2015. doi: 10.1371/journal.pone.0131408
- [9] H. Wang, J. Peng, C. Xie, Y. Bao, and Y. He, "Fruit quality evaluation using spectroscopy technology: a review," Sensors, vol. 15, pp. 11889-11927, 2015.
- [10] B. Kashyap and R. Kumar, "A plug-and-play type field-deployable bio-agent-free salicylic acid sensing system," IEEE Sensor Journal, vol. 21, no. 21, pp. 24820-24828, 2021.
- [11] B. Kashyap and R. Kumar, "Sensing methodologies in agriculture for monitoring biotic stress in plants due to pathogens and pests," Inventions, vol. 6, pp. 29, 2021.
- [12] N. I. Hossain and S. Tabassum, "Stem-FIT: a microneedle-based multi-parametric sensor for in situ monitoring of salicylic acid and pH levels in live plants," in Proc. IEEE International Conference on Nano/Micro Engineered and Molecular Systems (NEMS), pp. 14-17, April 2022. DOI: 10.1109/NEMS54180.2022.9791212
- [13] N. I. Hossain and S. Tabassum, "Leaf-mounted microneedle-based multisensory platform for multiplexed monitoring of phytohormones in live plants," in Proc. Hilton Head Solid-State Sensors, Actuators, and Microsystems Workshop, June 5-9, 2022. [in press]
- [14] N. I. Hossain; T. Noushin, and S. Tabassum, "Leaf-FIT: a wearable leaf sensor for in-situ and real-time monitoring of plant phytohormones," in Proc. IEEE Sensors Conference, 31 Oct. - 03 Nov. 2021. doi: 10.1109/SENSORS47087.2021.9639842.
- [15] X. Cao, X. Zhu, S. He, X. Xu, Y. Ye, and S. Gunasekaran, "Gold nanoparticle-doped three-dimensional reduced graphene hydrogel modified electrodes for amperometric determination of indole-3acetic acid and salicylic acid", Nanoscale, vol. 11, pp. 10247-10256, 2019
- [16] S. Tabassum, D. P. Kumar, and R. Kumar, "Copper complex-coated nanopatterned fiber-tip guided mode resonance device for selective detection of ethylene," IEEE Sensors J., vol. 21, pp. 17420-17429, 2021
- [17] B. Esser, J. M. Schnorr, and T. M. Swager, "Selective detection of ethylene gas using carbon nanotube-based devices: Utility in determination of fruit ripeness," Angew. Chem. Int. Ed., vol. 51, no. 23, pp. 5752–5756, Jun. 2012.
- [18] T. Noushin, N. I. Hossain, and S. Tabassum, "Kirigami-patterned highly stable and strain insensitive sweat pH and temperature sensors

- for long-term wearable applications," in Proc. IEEE Healthcare Innovations and Point of Care Technologies (HI-POCT) Conference, 10-11 March 2022 doi: 10.1109/HI-POCT54491.2022.9744070.
- [19] E. R. Martinez, M. D. G. Martinez, A. M. D. Martinez, L. P. Dias, C. Casanova, E. Soler, M. R. Figas, M. D. Raigon, M. Plazas, S. Soler, and J. Prohens, "Fruit composition profile of pepper, tomato, and eggplant varieties grown under uniform conditions," Food Research International, vol. 147, pp. 110531, 2021.
- [20] L. Norberg, M. Hellman, K. Berglund, S. Hallin, and O. Berglund, "Methane and nitrous oxide production from agricultural peat soils in relation to drainage level and abiotic and biotic factors," Front. Environ. Sci., vol. 9, pp. 631112, 2021.
- [21] A Wiorek, M. Parrilla, M. Cuartero, and G. A. Crespo, "Epidermal patch with glucose biosensor: pH and temperature correction toward more accurate sweat analysis during sport practice," Anal. Chem., vol. 92, pp. 10153-10161, 2020.